IEEE Access
Multidisciplinary ⋮ Rapid Review ⋮ Open Access Journal

Received June 20, 2021, accepted July 11, 2021, date of publication July 16, 2021, date of current version August 5, 2021.

Digital Object Identifier 10.1109/ACCESS.2021.3097750

Efficient Multi-Port Bidirectional Converter With Soft-Switching Capability for Electric Vehicle Applications

RASOUL FARAJI[1], (Member, IEEE), LEI DING[1], (Senior Member, IEEE), TOHID RAHIMI[1], (Member, IEEE), HOSEIN FARZANEHFARD[2], (Member, IEEE), HOSSEIN HAFEZI[3], (Member, IEEE), AND MOHAMMAD MAGHSOUDI[2], (Member, IEEE)

[1]Key Laboratory of Power System Intelligent Dispatch and Control, School of Electrical Engineering, Shandong University, Ministry of Education, Jinan 250061, China
[2]Department of Electrical and Computer Engineering, Isfahan University of Technology, Isfahan 84156-83111, Iran
[3]Faculty of Information Technology and Communications, Tampere University, 33720 Tampere, Finland

Corresponding author: Lei Ding (dinglei@sdu.edu.cn)

This work was supported in part by the China Postdoctoral Science Foundation under Grant 2019M662357 and Grant 2019M662356, and in part by the Project of Shandong Province New and Old Kinetic Energy Conversion.

ABSTRACT In this paper, to solve the hard-switching operation problem and the lack of existing a bidirectional power flow path from output to the energy storage device of the conventional three-port converter, a new soft-switched bidirectional multi-port converter is proposed. A large number of switches, different power flow paths which vary in each operating mode, and changing the outputs and their power levels are some of the challenges to provide soft-switching conditions in multi-port converters. In the proposed converter, by changing the topology of the conventional three-port converter, the bidirectional power exchangeability between ports is provided. Moreover, a soft-switching cell is added, which can operate independently from the output power levels. Less number of components with low volume is one of the important features of this multi-port converter. Due to the soft-switching operation of the proposed converter, the size of passive components and heat-sink is reduced. In addition, by the use of coupled inductors in the soft-switching cell, only one magnetic core is used and thus, single-stage power conversion is achieved and conduction loss is reduced. In this paper, the converter operating modes are presented, and design considerations are discussed. Finally, a 200 W-200 V prototype is implemented, and the theoretical analysis is validated by the experimental results.

INDEX TERMS Multi-port converter, dc-dc converter, soft-switching, electric vehicle, hybrid power systems.

I. INTRODUCTION

Developments in technologies of power sources and energy storage devices and the demand to utilize varieties of sources in a specific system have led to the emergence of hybrid energy systems. Also, clean and renewable energies have received much more attention in recent years due to the problems associated with fossil fuels cause. In this regard, the usage trend of electric vehicles (EV) is rapidly growing. In the design of electric vehicles, the concepts of hybrid energy systems are used such that some sources with the ability of absorbing/generating power are utilized, and the sources exchange power with each other [1], [2].

In an electric vehicle, an energy generation source (EGS) like fuel cell, the energy storage systems (ESS) like battery and super-capacitor and a source with the ability to regenerate energy like regenerative braking system are utilized together. The power management between sources is handled by the power converters. Thus, a unidirectional converter for transferring power from EGS to load, and for transferring power from/to each of ESS and regenerate energy source (RES), a distinct bidirectional converter is needed [3].

By increasing the number of sources, more power converters must be employed, which leads to a higher number of components. Instead of using a dedicated converter for

The associate editor coordinating the review of this manuscript and approving it for publication was Tariq Masood.

each input source, a multi-port converter can be used [4], [5]. In this type of converters, different converters are integrated to reduce the number of components. For integration, some parts of the converter should be shared between different operating modes.

Multi-port converters operate in different operating modes. Depending on each operating mode, a port can act as an input or act as an output. Due to the use of different types of sources in EV applications, the inputs and outputs of the power converter in each operating mode are changed. Thus, the power flow paths are changed in each operating mode. Fig. 1 shows the different operating modes of a multi-port converter utilized in the EV application. The converter has six operating modes as briefly described below:

Mode I: In this mode, the generated power of EGS is more than load power demand, and ESS needs to be charged. Thus, a part of EGS generated power is transferred to the load, and the remained power is transferred to ESS.

Mode II: In this operating mode, ESS is fully charged, and the load is supplied by EGS.

Mode III: Load does not need to receive power, and EGS charges ESS.

Mode IV: The generated power of EGS is not enough to supply the load demand power, and ESS is used to compensate the lack of power.

Mode V: This operating mode happens when the load power demand increases instantaneously, and due to the faster response of the ESS than EGS, ESS supplies the load independently.

Mode VI: In this mode, the output port acts as a regenerative energy source and the generated power of this source is used to charge ESS.

In electric vehicle applications, the size and weight of the converter are very important factors. In most power converter topologies, inductors and heat-sinks have the most portion of the occupied volume and weight of the converter. Thus, the converter topologies must be utilized with the minimum number of inductors and small-size heat-sinks.

According to Fig.1, to implement each operating mode separately, the number of required inductors increases drastically. Thus, sharing converter inductors by different operating modes is a promising method to reduce the volume of the multi-port converters. Besides, by increasing the switching frequency, the size of passive components can be reduced. However, switching loss increases and imposes larger size heat-sinks to dissipate the heat [6], [7]. To meet the high switching frequency and mitigating the switching loss, soft-switching methods must be employed [8]. However, implementing soft-switching methods in multi-port converters is not a straightforward method [9], [10]. Different operating modes, changing the direction of the power flow paths, sharing the components, and large number of switches with different switching patterns are the challenges of implementing soft-switching techniques.

In literature, many non-isolated multi-port DC-DC converters are introduced, which have attempted to overcome some of the mentioned challenges. In [11], a family of integrated multi-port DC-DC converters with a reduced number of switches is presented. In this paper, the derived multi-port converter uses three switches, but three inductors are used that increase the converter volume. In addition, some switches operate under soft-switching condition in some operating modes, and fully soft-switching operation is not achieved. In [12], a three-port converter with the capability of charging ESS from EGS and output is presented. In this converter, all energies from various sources are accumulated in a DC-link and through a bidirectional converter, ESS is charged. In this converter, no components are shared such that three inductors are used that increase the size and volume of the converter. Also, power conversion is accomplished in more than one stage, which increases the conduction loss. In addition, the converter has four switches operating under the hard-switching conditions, which degrades the converter efficiency.

In [13]–[17], some power converters are introduced for utilizing in electric vehicle and hybrid electric vehicle applications. In [13], a multi-port converter is introduced that uses a simple switch-diode structure to add input sources. Also, through a single-inductor bidirectional converter, all sources can exchange power together. This converter uses three switches, but in order to extend the number of operating modes, three extra relays are utilized. In this converter, ESS cannot directly receive power from EGS and the switches operate under hard switching condition. In [15], [16], in order to derive a dual-input single-inductor converter, the bridge arrangement is used. In this arrangement, one switch and one of the input sources are placed in series which establish a branch. Then, the branches can be placed in series or parallel to derive a multi-input converter. In this method, all the power flow paths are shared between the input sources. The EV power systems normally use metal chassis and frames as the current return path. This requires most of the sources and loads to have a common ground port which the presented converters lack and do not meet the EV power systems requirements. Also, the mentioned converters do not operate under soft-switching. The multi-port converters introduced in [14], [17] dedicate a complete converter to transfer power from each input to the output. Thus, the component counts of these converters are high. In [14], four inductors and five switches and in [17], four inductors and six switches are used, which increase the design complexity of the converters. In [14], energy storage devices cannot be charged from other input sources, and the switches of both converters operate under hard-switching condition.

In [18], three boost converters are integrated to derive a multi-input converter. In this converter, one EGS and one ESS are used which the power flow paths from these inputs to the output are shared. Thus, a single inductor converter is achieved that reduces the converter size, and also the power conversion is done in a single stage for every operating mode. However, this converter does not have the ability to transfer power from the output to the ESS and thus, it is not applicable

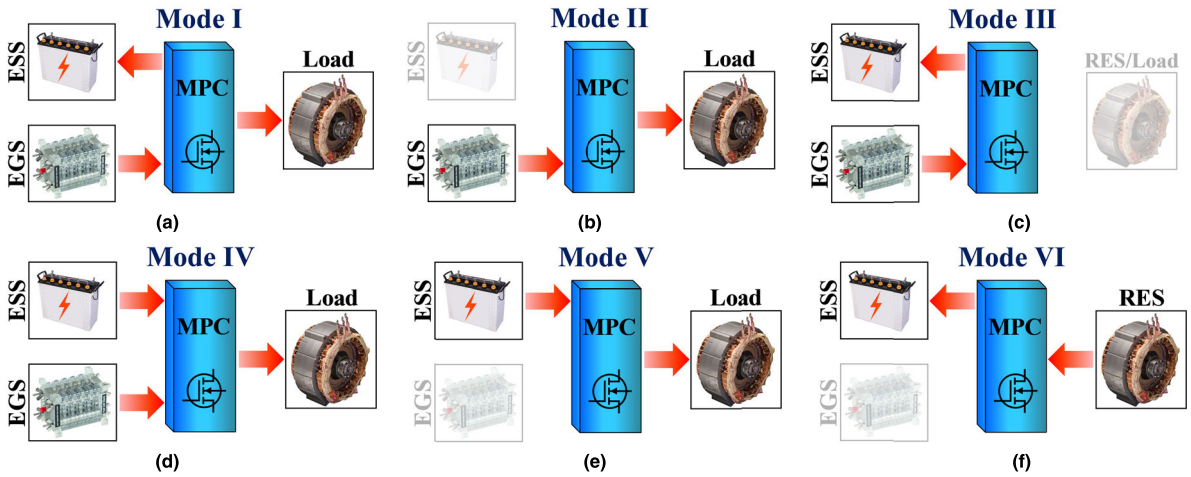

FIGURE 1. Different operating modes of a multi-port converter in EV application.

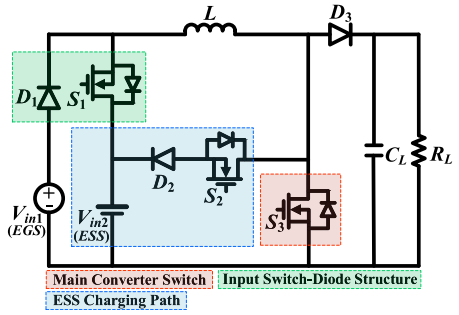

FIGURE 2. Conventional three-port converter (TPC).

to EV applications. The topology of this converter is shown in Fig. 2.

The topology of the introduced converter in [18] has been used as the base of many converters to derive a multi-input converter [19]–[23]. In [19], [20], the structure of conventional three-port converter (TPC) is changed to enhance the voltage gain. And to reduce the voltage stress on main switches, passive clamp circuits are used, but the switching loss still exists. In [21]–[23], some improvements are applied to the conventional TPC converter to provide soft-switching condition. A simple auxiliary resonant circuit is used in [21] to provide the soft-switching condition for the main switch and the switch in the ESS charging path. The auxiliary resonant circuit is integrated into the ESS charging path in which the resonance energy is recovered and sent to ESS. This converter has two inductors, and the converter volume is increased. Moreover, the switch in the input side operates under hard-switching condition. A passive lossless snubber circuit is presented in [22] to solve the hard-switching problem of the conventional TPC converter. In this converter, the pair of coupled-inductors along with an auxiliary inductor is used to provide turn-ON zero voltage switching (ZVS) and turn-OFF zero current switching (ZCS) conditions for the main switch. Also, the switch in the ESS charging path operates under ZCS. The hard-switching operation of the input switch and adding an extra magnetic core are the disadvantages of this converter. In [23], the TPC converter structure is changed and an active clamp circuit is added to provide soft-switching condition. In addition, the hard-switching problem of the input switch is solved, but the proper operation of the active clamp circuit is lost at low output power conditions and in some operating modes, soft-switching operation is missed. All of the introduced converters in [18]–[23] do not have the ESS charging capability from the output which limits their applications.

In this paper, to overcome the problems associated with the conventional TPC, including the hard-switching operation and disability of ESS charging from the output, a new soft-switched bidirectional multi-port DC-DC converter is proposed. To add the ESS charging ability from the output, a bidirectional power flow path is integrated into the TPC converter. And, to enhance the efficiency, a soft-switching cell with the minimum number of switches is added to the converter such that soft-switching condition for all switches in all operating modes is provided. By the use of coupled inductors in the soft-switching cell, the converter benefits from one magnetic core and all power conversions are done in a single-stage. As a result, both switching and conduction losses are reduced. The paper is organized in seven sections. The proposed converter and operating modes are described in section II. The converter design considerations are presented in section III. The experimental results are discussed in Section IV. In section V, efficiency and loss breakdown analysis are presented and the proposed topology is compared with some novel counterparts in section VI. Finally, the drawn conclusions from this manuscript are presented in section VII.

II. PROPOSED CONVERTER TOPOLOGY AND OPERATING MODES

The topology of the proposed soft-switched bidirectional multi-port converter (BTPC) is shown in Fig. 3. In this

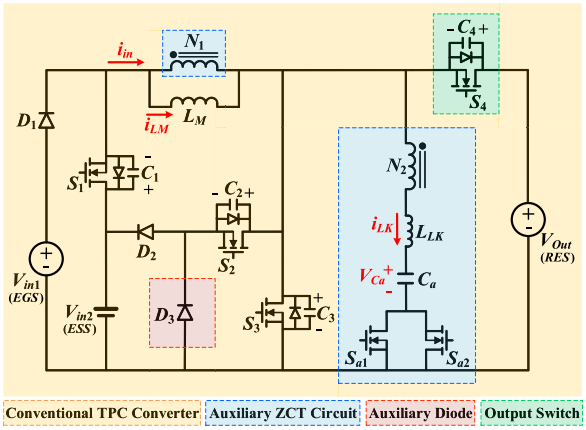

FIGURE 3. Proposed non-isolated soft-switched bidirectional multi-port DC-DC converter topology.

converter, the output diode in the conventional TPC is replaced by a switch (S_4) to provide a bidirectional power flow path between the ESS and the output. Then, snubber capacitors (C_1-C_4) are added to each switch to provide ZVS turn-OFF condition. Before the switches are turned ON, the snubber capacitors must be discharged to provide ZVS turn-ON condition for the switches. Therefore, a soft-switching cell is employed to discharge the snubber capacitors. To design and select a proper soft-switching cell, some points must be considered:

1- The BTPC has four switches, and to have a soft-switching operation for each switch, one soft-switching cell must be applied to each switch which increases the number of components drastically. Thus, a soft-switching technique must be used that can be shared to satisfy soft-switching condition for more than one switch.

2- The switches in BTPC are placed in different power flow paths. Moreover, the power flow paths are changed in different operating modes. To discharge the snubber capacitors and provide ZVS turn-ON condition, the snubber capacitors must be discharged through a reverse current to the ordinary direction. Especially for the switch in the input side, that the input current must be reversed in which it is very challenging. Also, C_2 discharging path is blocked by D_2.

3- In BTPC, the output ports are changed during the converter operation. According to Fig. 1, ESS and Load/RES in some modes act as input and in other modes act as output. Since the operation of some soft-switching circuits is dependent on the output power levels, selecting a proper soft-switching technique for BTPC is crucial.

4- In BTPC, at the worst condition, four snubber capacitors must be discharged during the soft-switching process and thus, the equivalent snubber capacitors value is large and the soft-switching cell must be able to provide enough energy to discharge them.

The soft-switching cell consists of coupled inductors (N_1, N_2 and the leakage inductance (L_{LK})), C_a and the auxiliary switches S_{a1} and S_{a2}. The magnetizing inductance (L_M) in coupled inductors acts as the main inductor of the converter and $n = N_2/N_1$. The leakage inductance in the soft-switching cell acts as the snubber inductor and provides ZCS turn-ON condition for S_{a1} and S_{a2}. Also, D_3 is added to deliver the discharging energy of C_2 and provide ZVS turn-ON condition for S_2.

In the proposed converter, V_{in1} is dedicated to energy generation sources like fuel cell, V_{in2} port is connected to an energy storage system like the battery or super-capacitor such that $V_{in2} > V_{in1}$. When S_1 is ON, D_1 is reverse biased and current just flows from V_{in2} and when S_1 is OFF, D_1 conducts and V_1 supplies the load. Through this simple switch-diode structure, power management between input sources can be easily done. And output port can be connected to a regenerative energy source or DC-link.

According to the power status of each source, the proposed multi-port converter has different operating modes indicated *in Fig. 1*. To simplify the converter analysis, it is assumed that the voltage of all sources is constant, all semiconductor components are ideal *and* the converter is at steady-state condition.

A. MODE I

In this operating mode, EGS supplies the required power of ESS and the output simultaneously. In other words, some amount of V_{in1} generated power is transferred to V_{out}, and the remaining power is delivered to V_{in2}. This operating mode has thirteen distinct operating intervals in each switching cycle. The key waveforms and the equivalent circuit of each interval are shown in Figs. 4 and 5, respectively. Prior to the first interval, it is assumed that all switches are OFF.

1) INTERVAL I ($t_0 - t_1$) [SEE FIG. 5(a)]

At the beginning of this interval, the body diode of S_4 conducts, and the stored energy in the magnetizing inductance is transferred to the output.

2) INTERVAL II ($t_1 - t_2$) [SEE FIG. 5(b)]

Before the switches turn ON, the corresponding snubber capacitors must be discharged. Thus, to provide ZVS turn-ON condition for the TPC switches, the soft-switching cell is activated. In this interval, S_{a1} is turned ON under ZCS condition due to leakage inductance. As a result, a constant positive voltage is applied to the leakage inductance through the coupled inductors, and its current (i_{LK}) increases linearly.

3) INTERVAL III ($t_2 - t_3$) [SEE FIG. 5(c)]

At t_2, the leakage inductance current becomes more than the output current and thus, the body diode of S_4 turns OFF. Then, a resonance begins between the leakage inductance and C_2-C_4 snubber capacitors. Thus, v_{C2} and v_{C3} decrease, and v_{C4} increases.

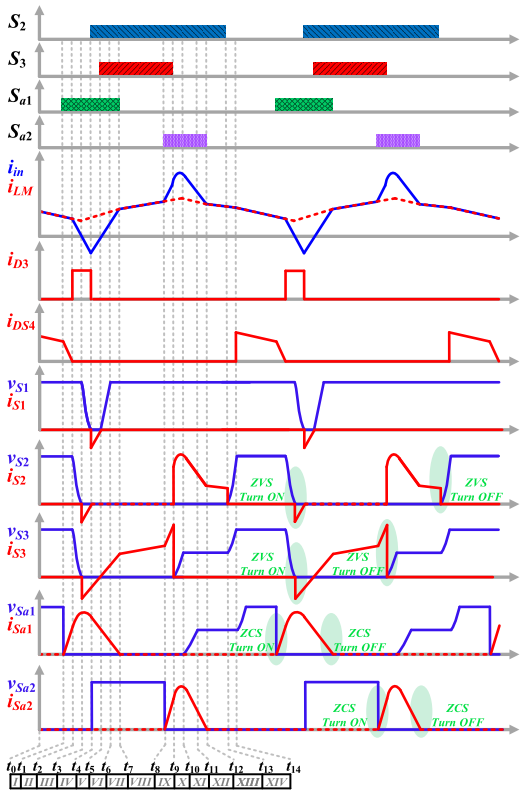

FIGURE 4. Key waveforms of the proposed converter in Mode I.

4) INTERVAL IV ($t_3 - t_4$) [SEE FIG. 5(d)]

This interval starts when C_4 is fully charged, and C_2 and C_3 are fully discharged. Therefore, the body diode of S_2 and S_3 conduct. During this interval, the direction of the input current is reversed, and a resonance occurs between leakage inductance and C_1 which causes C_1 to discharge. During this interval, i_{LK} starts to decrease.

5) INTERVAL V ($t_4 - t_5$) [SEE FIG. 5(e)]

When the body diode of S_3 is conducting, S_3 can turn ON under ZVS condition. In the meantime, v_{C1} reaches zero, and the body diode of S_1 conducts. Through the proposed soft-switching method and by the use of the ESS power flow path, the soft-switching energy is recovered and transferred to the ESS.

6) INTERVAL VI ($t_5 - t_6$) [SEE FIG. 5(f)]

At t_5, the direction of the input current becomes positive. Thus, the body diode of S_1 turns OFF, and the C_1 snubber capacitor is charged.

7) INTERVAL VII ($t_6 - t_7$) [SEE FIG. 5(g)]

This interval begins when C_1 is charged, and D_1 starts to conduct. Therefore, the magnetizing inductance is charged through V_{in1}.

8) INTERVAL VIII ($t_7 - t_8$) [SEE FIG. 5(h)]

At t_7, the leakage inductance current reaches zero, and S_{a1} turns OFF under ZCS condition. In this interval, the current in L_M continues to increase.

9) INTERVAL IX ($t_8 - t_9$) [SEE FIG. 5(i)]

In the previous intervals, a part of the stored energy in C_a is discharged, and in order to keep the voltage of this capacitor constant, S_{a2} is turned ON under ZCS condition due to L_{LK}. In this interval, a negative voltage is applied to the leakage inductance and i_{LK} decreases.

10) INTERVAL X ($t_9 - t_{10}$) [SEE FIG. 5(j)]

In order to charge ESS, S_3 is turned OFF under ZVS condition due to the snubber capacitor. Then, v_{C3} increases.

11) INTERVAL XI ($t_{10} - t_{11}$) [SEE FIG. 5(k)]

At t_{10}, v_{C3} reaches V_{in2} and D_2 conducts. Because the C_2 snubber capacitor was discharged during interval IV, S_2 is turned ON under ZVS condition. And the stored energy in L_M is transferred to ESS. Due to the induced voltage by the coupled inductors, i_{LK} decreases toward zero during this interval.

12) INTERVAL XII ($t_{11} - t_{12}$) [SEE FIG. 5(l)]

At the beginning of this interval, i_{LK} reaches zero, and S_{a2} is turned OFF under ZCS condition while *ESS* is charged by V_{in1}.

13) INTERVAL XIII ($t_{12} - t_{13}$) [SEE FIG. 5(m)]

At t_{12}, S_2 is turned OFF under ZVS due to C_2. Then, the voltage of C_2 and C_3 increase, and the voltage of C_4 decreases. At the end of this interval, C_4 is fully discharged, and the body diode of S_4 conducts. This interval is the last interval in a switching cycle in Mode I.

B. MODE II

In this operating mode, EGS just supplies the output demand power. The converter operation is approximately similar to Mode I, with the difference that S_2 never turns ON in this mode. Therefore, converter operation starts from intervals I to IX, then ends in Interval XIII (Figs. 5(a)-(i) plus Fig. 5 (m)).

C. MODE III

In this mode, all the generated power by EGS is used to charge ESS. This operating mode is similar to Mode I with the difference that S_2 is always ON and no power is transferred to the output port. By switching S_3, the power flow is controlled and similar to other operating modes, S_{a1} is activated before S_3 is turned ON and S_{a2} is activated after S_3 is turned-OFF to provide soft-switching condition for the S_3 switch.

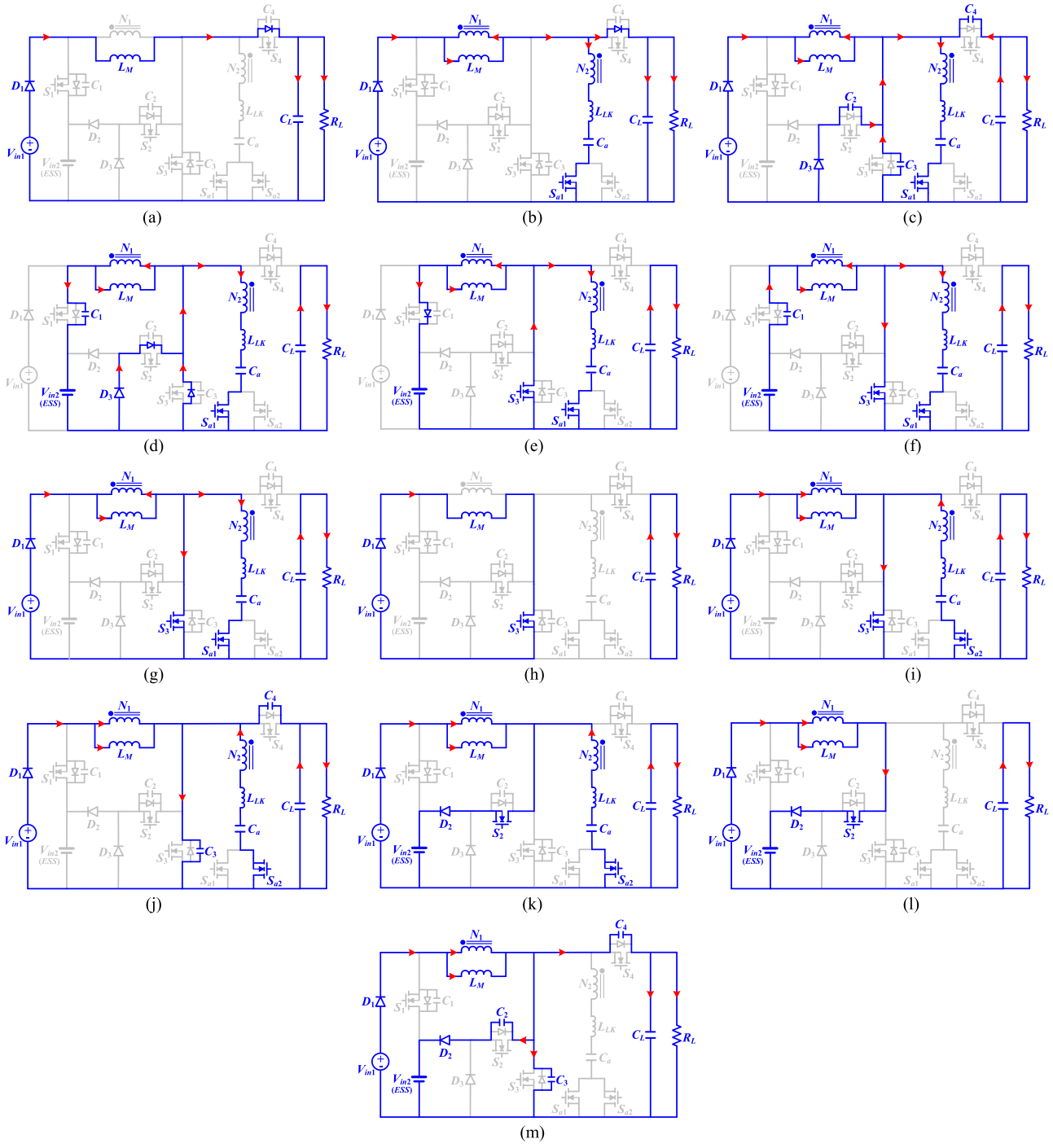

FIGURE 5. Proposed converter equivalent circuit in each interval for Mode I. (a) Interval I [t_0, t_1], (b) Interval II [t_1, t_2], (c) Interval III [t_2, t_3], (d) Interval IV [t_3, t_4], (e) Interval V [t_4, t_5], (f) Interval VI [t_5, t_6], (g) Interval VII [t_6, t_7], (h) Interval VIII [t_7, t_8], (i) Interval IX [t_8, t_9], (j) Interval X [t_9, t_{10}], (k) Interval XI [t_{10}, t_{11}], (l) Interval XII [t_{11}, t_{12}], (m) Interval XIII [t_{12}, t_{13}].

D. MODE IV

In this operating mode, both input sources supply the output load simultaneously. And, S_1 is switched such that the harvested energy from each input is controlled. This operating mode has thirteen distinct intervals in each switching cycle. The key waveforms and the equivalent circuit of each interval are shown in Figs. 6 and 7, respectively. Prior to the first interval, it is assumed that S_1, S_3 and S_{a1} are ON and S_2, S_4 and S_{a2} are OFF, and the leakage inductance current is decreasing.

1) INTERVAL I ($t_0 - t_1$) [SEE FIG. 7(a)]

In this interval, S_1 and S_3 are ON, and L_M is being charged by V_{in2}.

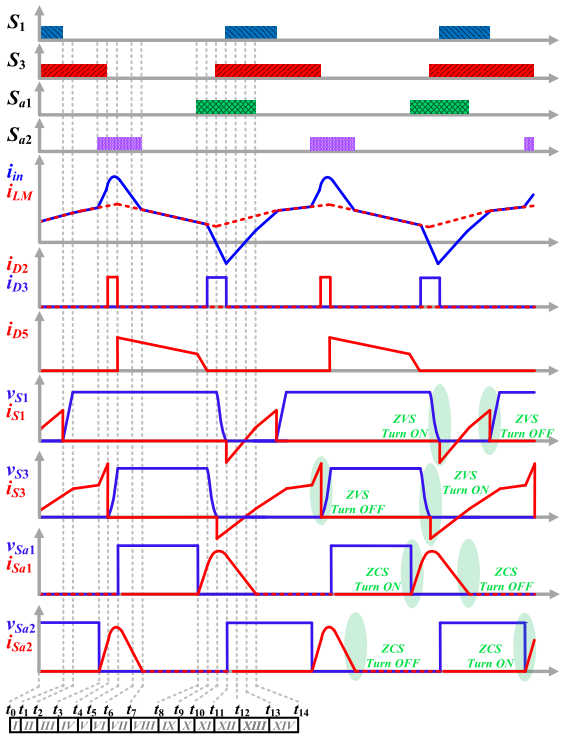

FIGURE 6. Key waveforms of the proposed converter in Mode IV.

2) INTERVAL II ($t_1 - t_2$) [SEE FIG. 7(b)]

To receive power from V_{in1}, S_1 is turned OFF under ZVS due to C_1 snubber capacitor, and v_{C1} is increased.

3) INTERVAL III ($t_2 - t_3$) [SEE FIG. 7(c)]

At t_2, the C_1 voltage reaches the difference of input voltage sources, and D_1 starts to conduct. Thus, L_M is being charged by V_{in1}.

4) INTERVAL IV ($t_3 - t_4$) [SEE FIG. 7(d)]

In this interval, S_{a2} is turned ON to charge C_a. The S_{a2} turn-ON operation is under ZCS condition due to the leakage inductance.

5) INTERVAL V ($t_4 - t_5$) [SEE FIG. 7(e)]

At the beginning of this interval, S_3 is turned OFF under ZVS condition. Then, the voltage of C_2 and C_3 increase, and the voltage of C_4 decreases through a resonance with the leakage inductance.

6) INTERVAL VI ($t_5 - t_6$) [SEE FIG. 7(f)]

At t_5, v_{C4} reaches zero and the body diode of S_4 starts to conduct. The magnetizing inductance is supplying energy to the load. Also, the current through the leakage inductance decreases.

7) INTERVAL VII ($t_6 - t_7$) [SEE FIG. 7(g)]

At t_6, i_{LK} reaches zero, and S_{a2} is turned OFF under ZCS condition.

8) INTERVAL VIII ($t_7 - t_8$) [SEE FIG. 7(h)]

To discharge the C_1-C_3 snubber capacitors and to provide ZVS turn-ON condition, S_{a1} is turned ON. Since the S_{a1} current rate is restricted by the leakage inductance, this switch is turned ON under ZCS condition. Also, due to the positive voltage induced on L_{LK}, i_{LK} is increasing.

9) INTERVAL IX ($t_8 - t_9$) [SEE FIG. 7(i)]

This interval begins when i_{LK} becomes more than the output current, and the body diode of S_4 turns OFF under ZCS condition. Then, a resonance occurs between the leakage inductance and C_2-C_4, and v_{C2} and v_{C3} decrease and v_{C4} increases.

10) INTERVAL X ($t_9 - t_{10}$) [SEE FIG. 7(j)]

At the beginning of this interval, C_2 and C_3 are fully discharged, and the corresponding body diodes start to conduct. During this interval, the input current direction becomes negative, and D_1 turns OFF. Then, the voltage of C_1 decreases through a resonance with L_{LK}.

11) INTERVAL XI ($t_{10} - t_{11}$) [SEE FIG. 7(k)]

At the beginning of this interval, S_3 is turned ON under ZVS and C_1 is discharged, and the body diode of S_1 turns ON.

12) INTERVAL XII ($t_{11} - t_{12}$) [SEE FIG. 7(l)]

When the body diode of S_1 is conducting, S_1 can be turned ON under ZVS condition.

13) INTERVAL XIII ($t_{12} - t_{13}$) [SEE FIG. 7(m)]

At t_{12}, the input current direction is reversed, and at t_{13}, the current through S_{a1} becomes zero. Thus, S_{a1} can be turned OFF under ZCS condition.

E. MODE V

In this operating mode, ESS supplies the output load independently. The converter operation in this mode is similar to Mode IV with the difference that S_1 is always ON and D_1 is always OFF. In this mode, just S_3 is switched. Similar to other operating modes, S_{a1} and S_{a2} are switched such that the soft-switching condition for S_3 is provided.

F. MODE VI

In the previous operating modes, the output port acted as the power sink and absorbed power from the other ports. However, in mode VI, the output port acts as a power source and the generated power in this port is used to charge ESS. This operating mode has eleven distinct operating intervals in each switching cycle. The key waveforms and the equivalent circuit of each interval are shown in Figs. 8 and 9, respectively. Prior to the first interval, it is assumed that S_1, S_4 and S_{a2} are ON and other switches are OFF and the leakage inductance current is decreasing.

1) INTERVAL I ($t_0 - t_1$) [SEE FIG. 9(a)]

This interval starts when the leakage inductance current reaches zero. During this interval, the magnetizing inductance is charged by V_{out}.

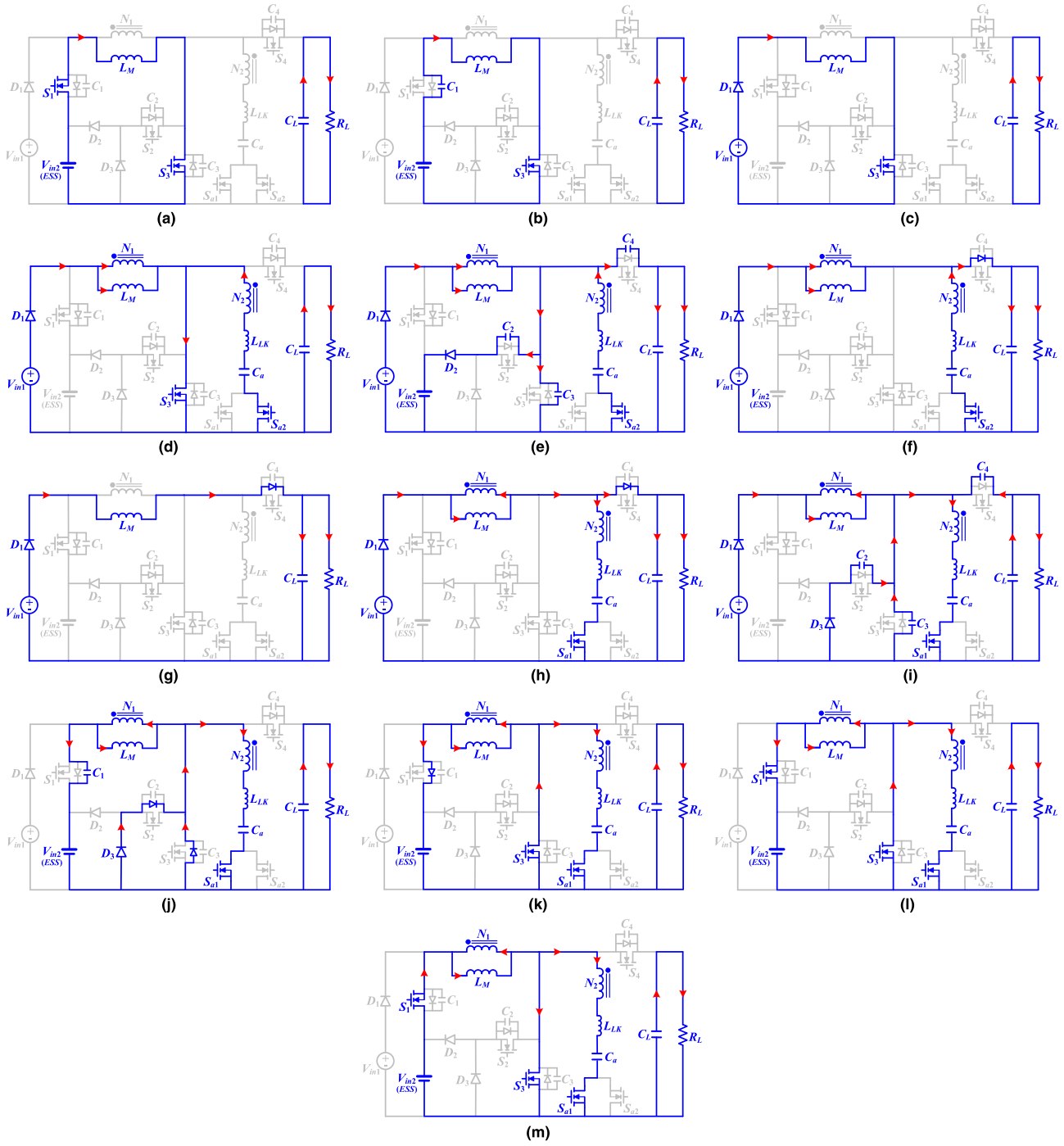

FIGURE 7. Proposed converter equivalent circuit in each interval for Mode IV. (a) Interval I [t_0, t_1], (b) Interval II [t_1, t_2], (c) Interval III [t_2, t_3], (d) Interval IV [t_3, t_4], (e) Interval V [t_4, t_5], (f) Interval VI [t_5, t_6], (g) Interval VII [t_6, t_7], (h) Interval VIII [t_7, t_8], (i) Interval IX [t_8, t_9], (j) Interval X [t_9, t_{10}], (k) Interval XI [t_{10}, t_{11}], (l) Interval XII [t_{11}, t_{12}], and (m) Interval XIII [t_{12}, t_{13}].

2) INTERVAL II (t_1 – t_2) [SEE FIG. 9(b)]

In this interval, to charge C_a, S_{a1} is turned ON at ZCS due to series L_{LK}.

3) INTERVAL III (t_2 – t_3) [SEE FIG. 9(c)]

At t_2, S_4 is turned OFF under ZVS condition, and its corresponding snubber capacitor is charged. In the meantime, C_2 and C_3 are discharged in a resonance interaction with the leakage inductance.

4) INTERVAL IV (t_3 – t_4) [SEE FIG. 9(d)]

At t_3, v_{C2} and v_{C3} reach zero, and the body diodes of S_2 and S_3 start to conduct. During this interval, i_{LK} is decreasing.

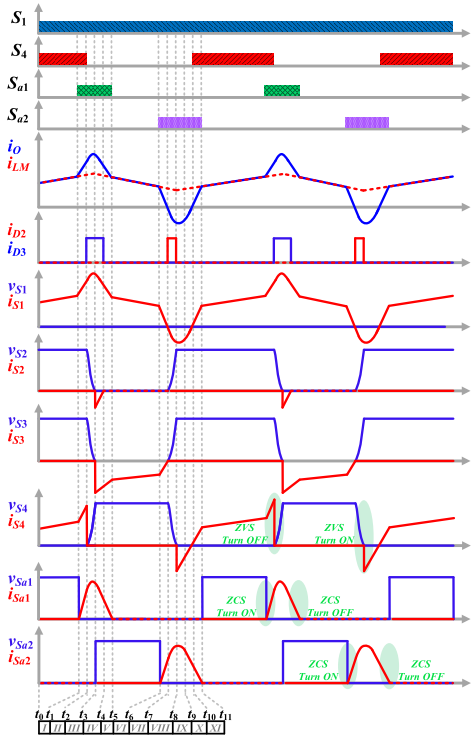

FIGURE 8. Key waveforms of the proposed converter in Mode VI.

5) INTERVAL V (t_4 – t_5) [SEE FIG. 9(e)]

In this interval, i_{LK} is still decreasing, and i_{LM} passes through the body diode of S_3.

6) INTERVAL VI (t_5 – t_6) [SEE FIG. 9(f)]

At t_6, the leakage inductance current reaches zero, and S_{a1} is turned OFF under ZCS condition.

7) INTERVAL VII (t_6 – t_7) [SEE FIG. 9(g)]

To provide soft-switching condition for S_4, S_{a2} is turned ON. Then, i_{LK} increases in the reverse direction.

8) INTERVAL VIII (t_7 – t_8) [SEE FIG. 9(h)]

In this interval, the current through N_1 becomes more than i_{LM} and in a resonance process between C_2-C_4 with L_{LK}, v_{C2} and v_{C3} increase, and v_{C4} decreases.

9) INTERVAL IX (t_8 – t_9) [SEE FIG. 9(i)]

When v_{C4} reaches zero, the body diode of S_4 conducts and i_{LK} decreases.

10) INTERVAL X (t_9 – t_{10}) [SEE FIG. 9(j)]

When S_4 body diode is conducting, S_4 can be turned ON under ZVS condition.

11) INTERVAL XI (t_{10} – t_{11}) [SEE FIG. 9(k)]

At t_{10}, the coupled inductors primary side current becomes lower than i_{LM}. This interval ends when i_{LK} becomes zero and S_{a2} is turned OFF under ZCS condition.

III. CONVERTER ANALYSIS AND DESIGN CONSIDERATIONS

In this section, the analysis of the proposed bidirectional TPC is investigated, and the voltage gain, inductor design, and soft-switching conditions are discussed. To simplify the analysis, it is assumed that the voltage across C_a is constant, all circuit elements are ideal, and the converter operates under steady-state condition. In this section, d_{S1}, d_{S2}, d_{S3} and d_{S4} are used to indicate the duty cycle of switches S1, S2, S3 and S4, respectively.

In Fig. 10, the operating modes selection of the proposed converter is illustrated.

A. VOLTAGE GAINS

According to the operating modes shown in Fig.1, the proposed converter has six different voltage gains:

1) MODE I

In this mode, V_{in1} supplies the demand power of V_{in2} and V_{out} simultaneously. Using the volt-second balance principle on the magnetizing inductance as (1), the voltage gain can be achieved by (2):

$$d_{S3}V_{in1} = d_{S2}(V_{in2} - V_{in1}) + (1 - d_{S2} - d_{S3}) \times (V_{out} - V_{in1}) \quad (1)$$

$$V_{Out} = \frac{1}{1 - (d_{S2} + d_{S3})}[V_{in1} - d_{S2}V_{in2}] \quad (2)$$

2) MODE II AND MODE V

In these operating modes, each of V_{in1} and V_{in2} supplies output power separately. By considering $V_{in1} = V_{in2} = V_{IN}$ the voltage gains of mentioned operating modes are the same. Equation (3) indicates the magnetizing volt-second balance principle applied on magnetizing inductance which results the voltage gain presented by equation (4).

$$d_{S3}V_{IN} = (1 - d_{S3})(V_{out} - V_{IN}) \quad (3)$$

$$\frac{V_o}{V_{IN}} = \frac{1}{1 - d_{S3}} \quad (4)$$

3) MODE III

The whole generated power of V_{in1} is transferred to V_{in2}. Thus, V_{in2} in this mode acts as the output. By applying the volt-second balance principle on L_M (5), the voltage gain is achieved (6).

$$d_{S3}V_{in1} = (1 - d_{S3})(V_{in2} - V_{in1}) \quad (5)$$

$$\frac{V_{in2}}{V_{in1}} = \frac{1}{1 - d_{S3}} \quad (6)$$

4) MODE IV

In this mode, V_{in1} and V_{in2} contribute to the volt-second balance principle calculation of magnetizing inductance (7), results in the voltage gain can be calculated by (8).

$$d_{S1}V_{in2} + (d_{S3} - d_{S1})V_{in1} = (V_{out} - V_{in1})(1 - d_{S3}) \quad (7)$$

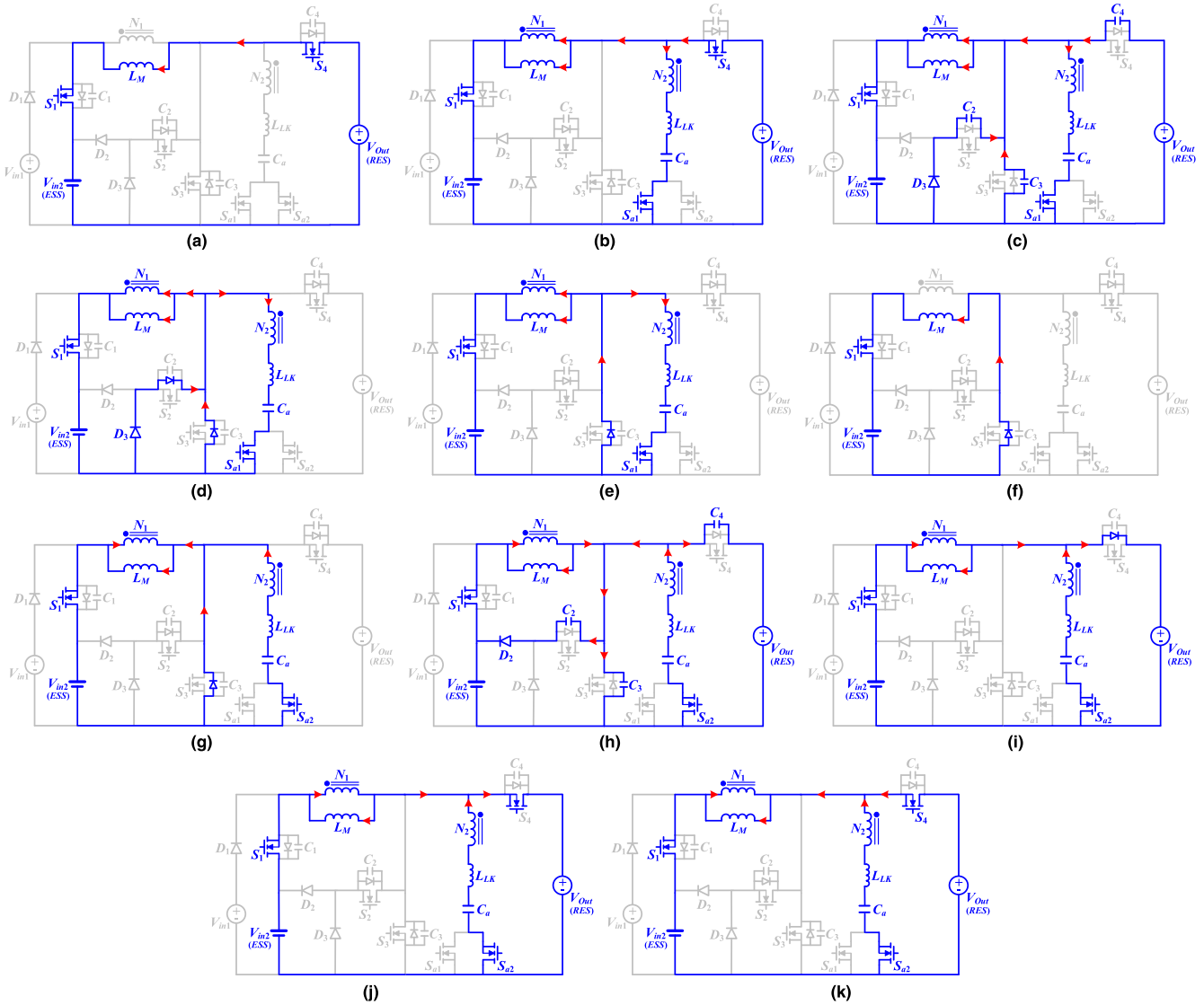

FIGURE 9. Proposed converter equivalent circuit in each interval for Mode IV. (a) Interval I [t_0, t_1], (b) Interval II [t_1, t_2], (c) Interval III [t_2, t_3], (d) Interval IV [t_3, t_4], (e) Interval V [t_4, t_5], (f) Interval VI [t_5, t_6], (g) Interval VII [t_6, t_7], (h) Interval VIII [t_7, t_8], (i) Interval IX [t_8, t_9], (j) Interval X [t_9, t_{10}], and (k) Interval XI [t_{10}, t_{11}].

$$V_{out} = \frac{1}{1 - d_{S3}} \times \left[(1 - d_{S1}) V_{in1} + d_{S1} V_{in2} \right] \tag{8}$$

5) MODE VI

During this mode, the V_{out} acts as the power source, and the generated power of V_{out} is transferred to V_{in2}. In this mode, just S_4 is switched. Equation (9) shows the volt-second balance principle of magnetizing inductance and equation (10) indicates the derived voltage gain for this mode:

$$d_{S4}(V_{out} - V_{in2}) = (1 - d_{S4}) V_{in2} \tag{9}$$

$$\frac{V_{in2}}{V_{out}} = d_{S4} \tag{10}$$

Fig. 11 depicts the voltage gain curves of each operating mode.

B. INDUCTOR DESIGN

In the proposed converter, the magnetizing inductance of the coupled inductors is shared between all operating modes. The converter is designed to operate in continuous conduction mode (CCM). Thus, the optimum value of the magnetizing inductance must be selected. The proposed converter in Modes I-V acts as the boost converter. In these modes, the magnetizing inductance value can be calculated as follows:

$$i_{LM_{(Avg)}} = \frac{2 \cdot I_o}{(1 - d_{S1})} \tag{11}$$

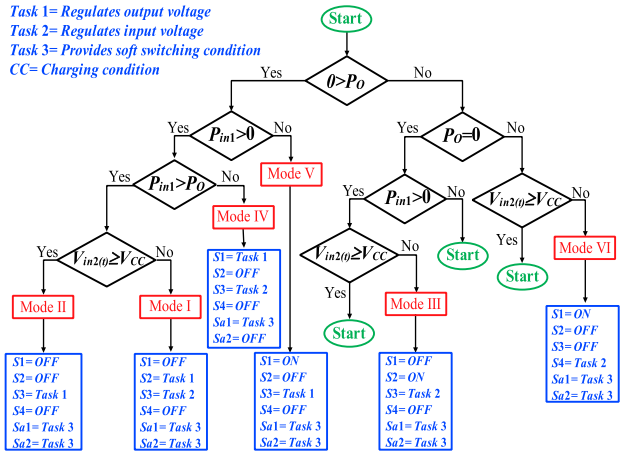

FIGURE 10. Operating modes selection flow chart for the proposed converter.

$$\Delta i_{LM} = \frac{d_{S1} \cdot V_{IN}}{L_M \cdot f_s} \tag{12}$$

$$L_M \geq \frac{d_{S1} \cdot (1 - d_{S1})^2 \cdot V_{O\_mode}^2}{2 \cdot f_s \cdot P_{O\_mode(Critical)}} \tag{13}$$

where $i_{LM(avg)}$ is the average value and Δi_{LM} is the ripple of L_M current so that by substituting (12) into (11) and using (1)-(6), the minimum value of L_M at the boundary of CCM and DCM is achieved (13). In equation (13), V_{O_mode} refers to the output voltage of each operating mode, and $P_{O\_mode(Critical)}$ is the minimum power in which for a specific value of L_M, the converter operates in the boundary of CCM and DCM.

In Mode VI, the proposed converter operates as a buck converter and similar calculations can be done for this mode:

$$i_{LM_{(Avg)}} = \frac{2 \cdot P_{Vin2}}{V_{in2}} \tag{14}$$

$$\Delta i_{LM} = \frac{(1 - d_{S4}) \cdot V_{in2}}{L_M \cdot f_s} \tag{15}$$

By substituting (15) into (14), the minimum value of magnetizing inductance at the boundary of CCM and DCM is achieved as:

$$L_M \geq \frac{(1 - d_{S4}) \cdot V_{in2}^2}{2 \cdot f_s \cdot P_{Vin2(Critical)}} \tag{16}$$

C. SOFT-SWITCHING CONDITIONS

The principle of soft-switching operation of the proposed converter is investigated in this section. Before main switches become turn ON, the auxiliary switches must be turned ON to provide ZVS condition. At the first step, one of the auxiliary switches is activated, then the summation of output voltage and V_{Ca} and the secondary side voltage of coupled inductors is drooped on the leakage inductance. Then, the i_{LK} starts to increase linearly until it reaches i_{out}. Then, through a resonance process, the snubber capacitors are discharged. Thus, in order to have soft-switching conditions, the following points must be satisfied.

1) PROVIDING ZVS TURN-OFF CONDITION FOR S_1, S_2, S_3 AND S_4

$C1$-$C4$ snubber capacitors provide zero voltage switching condition for their corresponding switches at turn-OFF instant. Therefore, their minimum value can be selected similar to any snubber capacitor as follow [24]:

$$C_{1-4} \geq C_{min} = \frac{I_{sw} t_f}{2 V_{sw}} \tag{17}$$

where I_{SW} is the switch current before switch turn-OFF instant, t_f is the switch current fall time, and V_{SW} is the switch voltage after turn-OFF.

2) PROVIDING ZCS TURN-ON CONDITION FOR S_{a1} AND S_{a2}

Leakage inductance acts as the snubber inductor at turn-ON instant of the auxiliary switches. The minimum value of snubber inductor can be defined as:

$$L_{Leakage} \geq L_{Leakage\_min} = \frac{V_{sw} t_r}{2 I_{sw}} \tag{18}$$

where V_{SW} is switch voltage before switch turns ON, t_r is the switch current rise time, and I_{SW} is the switch current after switch turns ON.

3) PROVIDING ZVS TURN-ON CONDITION FOR MAIN SWITCHES

To obtain the ZVS condition at turn-ON instant of the TPC switches, the voltage of the switches must reach zero. The soft-switching condition in operating modes I to VI are almost the same. Thus, as an example, just the soft-switching condition for Mode V is investigated in this section. During intervals III and IV, the snubber capacitors through resonance by leakage inductance are discharged. To simplify calculations, it is assumed that the value of all snubber capacitors are the same such that $C_1 = C_2 = C_3 = C_4 = C_S$, and they are discharged at the same time. The simplified resonance equation is presented as follows (19)–(24), as shown at the bottom of the next page:

To calculate the value of V_{Ca} some simplifications are necessary; otherwise, the relations would become cumbersome. According to (19)-(24), the first soft-switching condition is achieved as follow:

$$V_{Ca} \geq V_{IN} - \frac{V_{out}}{4} \tag{25}$$

Assuming that the resonance time is short enough to omit it in comparison with the switching period. Fig. 12 shows the simplified waveform of i_{Ca} at the steady-state condition which the average of i_{Ca} would be zero. Thus, the value of V_{Ca} can be obtained as follow:

$$V_{Ca} = V_{\text{out}} (n + 1) - n V_{IN} - \frac{I_{LM} L_{LK}}{n t_{3-4}} \tag{26}$$

where t_3-t_4 is the duration time of interval IV in Fig. 6 which would be adjustable and it can be expressed as follow:

$$t_{3-4} = \frac{2 I_{LM} L_{LK}}{V_{\text{out}} (2n + 1) - 2 n V_{IN}} \tag{27}$$

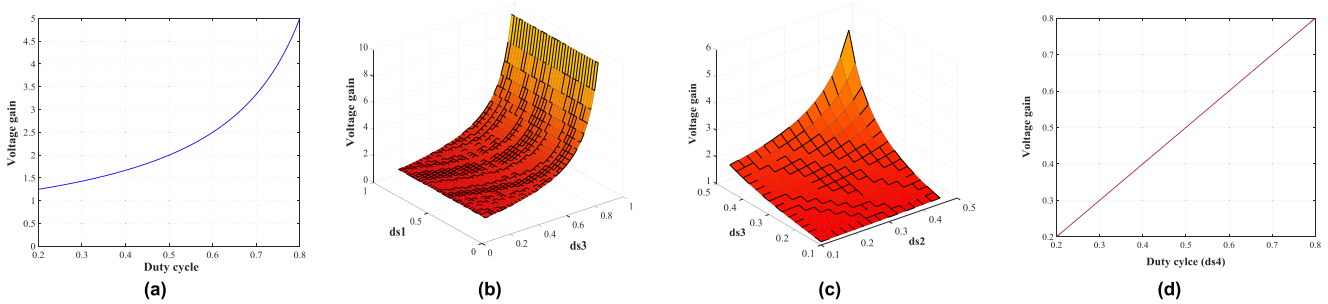

FIGURE 11. Voltage gain graphs in different modes. (a) Modes II, III, and V. (b) Mode IV (VA = VB). (c) Mode I (VA = VB). (d) Mode VI.

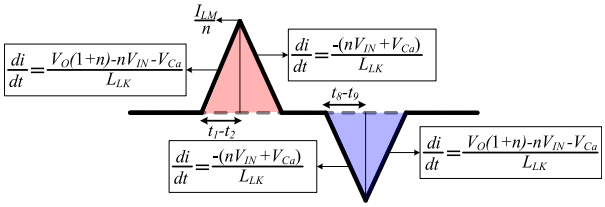

FIGURE 12. Simplified waveform of i_{Ca}.

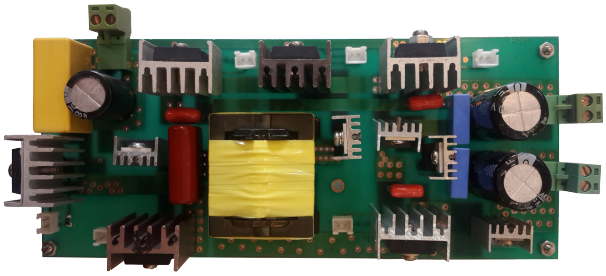

FIGURE 13. Photograph of the implemented prototype.

Before main switches of the converter would turn ON, auxiliary switches must be turned ON to discharge the snubber capacitors and to provide ZVS condition. Thus, t_{ZVT} is the minimum required time which auxiliary switches must be turned ON before main switches become active and is defined by:

$$t_{\mathrm{ZVT}} = \frac{1}{\omega_1}\left[\cos^{-1}\left\{\frac{A_1}{\sqrt{B_1^2+C_1^2}}\right\}+\tan^{-1}\left(\frac{B_1}{C_1}\right)\right] \quad (28)$$

The t_{ZVT} must be shorter than the OFF time of the main converter switch in each mode:

$$t_{\mathrm{ZVT}} \le \left[1-d_{S\_mode}\right] T_{\mathrm{SW}} \quad (29)$$

4) PROVIDING ZCS TURN-OFF CONDITION

During soft-switching process, the auxiliary switches must be kept ON enough in order to the leakage inductance current reaches zero and ZCS condition achieves. The t_{ZCT} is defined by Equation (30):

$$t_{ZCT} = \frac{I_{Lk}\,(t_4)\,L_{LK}}{V_O(1+n)-nV_{IN}-V_{Ca}} + t_{ZVT} + \frac{3I_{Lk}\,(t_6)\,L_{LK}}{(nV_{IN}+V_{Ca})} \quad (30)$$

IV. EXPERIMENTAL RESULTS

To verify the effectiveness of the proposed converter, the prototype of the converter is implemented to supply a 200 W–200 V load. The specifications of the prototype are indicated in Table 1 and the photograph of the converter prototype is shown in Fig. 13. Also, experimental waveforms are shown in Fig. 14. Fig.14 (a)-(c) shows the waveforms of active switches in mode V. As it is shown in Fig 14(a),

$$v_{CS}\,(t) = A_1 + B_1 \sin\omega_1\,(t-t_{r1}) + C_1 \cos\omega_1\,(t-t_{r1}) \quad (19)$$

$$A_1 = \frac{V_{IN}n\,(1+n) - V_{Ca}\,(1+n) + 3V_O n^2}{4n^2+2n+1} \quad (20)$$

$$B_1 = \frac{[I_{LM}\,(t_{r1-1})\,(4n^2+5n+1)] - [i_{LK}\,(t_{r1-1})\,(4n^3+5n^2+3n+1)]}{Z_1} \quad (21)$$

$$C_1 = \frac{V_O(n^2+2n+1) + V_{Ca}\,(1+n) - V_{IN}n\,(1+n)}{4n^2+2n+1} \quad (22)$$

$$Z_1 = \frac{\sqrt{L_{LK}}}{(4n^2+2n+1)\sqrt{3C_S(4n^2+2n+1)}} \quad (23)$$

$$\omega_1 = \frac{4n^2+2n+1}{\sqrt{C_S L_{LK}}} \quad (24)$$

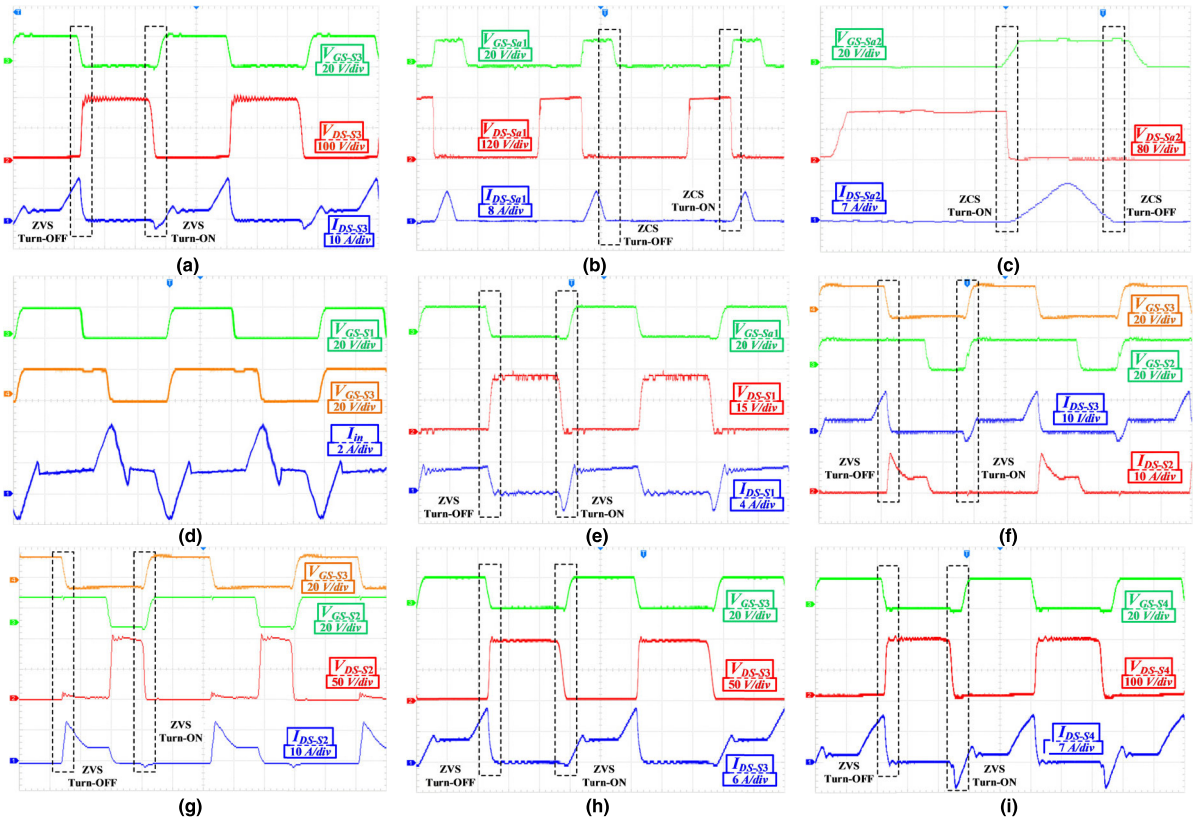

FIGURE 14. Waveforms of the implemented prototype in different operating modes: (a), (b) and (c) Mode V. (d) and (e) Mode IV. (f) and (g) Mode I. (h) Mode III. (i) Mode VI. [All time scales are 2 μS/div except (c) which is 1 μS/div].

TABLE 1. Key parameters of the implemented prototype.

Symbol	Parameter	Value
L_M	Magnetizing inductance	650 µH
N	Turns ratio	0.4
C_L	Output capacitors	10 µF
C_1-C_3	Snubber capacitors	3 nF
D_1-D_5	Diodes	MUR1640
S_1-S_4	Switches	IRF250P225
S_{a1}-S_{a2}	Switches	TK31N60W
f_S	Switching frequency	100 kHz
V_1	EGS (Unidirectional fixed voltage Source)	70 V
V_2	ESS	96 V
V_o	Output voltage	200 V

the S_3 main switch operates under ZVS condition. Also, Figs 14 (b)-(c) show that axillary switches operate under ZCS condition. The waveforms of S_3 in mode II are the same as Fig. 14(a), and for all operating modes, the waveforms of S_{a1} and S_{a2} are almost similar to Figs 14 (b)-(c). In mode IV, both EGS and ESS must contribute to supply the load. Thus, S_1 is switched to control the received power from each source. To provide ZVS condition for $S1$, the soft-switching cell must be able to reverse the direction of the input current. Accordingly, Fig. 14 (d) indicates that the input current direction is reversed. Thus, the S_1 switch operates under ZVS condition, as shown in Fig. 14 (e). In mode I, some amounts of stored energy in magnetizing inductance must be transferred to the load, and the remained energy must be transferred to ESS. This is done by adjusting the activation time of S_2 switch which is shown in Fig. 14 (f). In this mode, S_2 operates under ZVS condition (Fig. 14 (g)). In mode III, EGS charges ESS and S_3 control this mode. The ZVS operation of S_3 in this mode is shown in Fig. 14 (h). In mode VI, S_4 is activated such that how ESS is charged through output. In this mode, S_4 is switched under the ZVS condition (Fig. 14 (i)).

V. EFFICIENCY AND LOSS BREAKDOWN ANALYSIS

In this section, the experimental results are used to investigate the efficiency of the proposed converter in all operating modes and wide range of output power. Also, the components loss breakdown analysis at full load condition is analyzed. In mode I, half of the EGS generated power is transferred to the output load, and the remaining power is transferred to the ESS. And in mode IV, each input source supplies the load with the same amount of power. In Fig. 15 the efficiency of the proposed converter is compared with the conventional three-port converter (Fig. 2). According to the results, it can conclude that by reducing the switching loss through using the proposed soft-switching method, the efficiency is enhanced in a wide range of the output power. Also, the detailed loss analysis of the main components is shown in Fig.16 which

TABLE 2. Features comparison of multi-port converters with the proposed converter.

Converters	Converter topology type	No. of switches	No. of diodes	No. of Magnetic Cores	Six modes & Fully soft-switched	Operating modes (N/A: Not available, Soft Switching: ✓, Hard switching: ×)					
						Mode I	Mode II	Mode III	Mode IV	Mode V	Mode VI
[9]	Other	4	5	2	×	✓	✓	✓	✓	✓	N/A
[12]	Other	4	4	3	×	×	×	×	×	×	×
[17]	Other	6	2	4	×	×	×	×	×	×	×
[19]	TPC-based	3	5	2	×	×	×	×	×	×	N/A
[20]	TPC-based	3	8	1	×	×	×	×	×	×	N/A
[21]	TPC-based	3	5	2	×	✓	✓	×	×	✓	N/A
[22]	TPC-based	3	7	2	×	✓	✓	×	×	✓	N/A
[25]	TPC-based	4	5	1	×	✓	✓	✓	✓	✓	N/A
[26]	Other	5	0	2	×	✓	✓	N/A	✓	✓	N/A
[27]	Other	3	2	5	×	N/A	✓	N/A	✓	✓	N/A
[28]	Other	4	3	1	×	✓	✓	×	✓	✓	N/A
[29]	Other	6	0	2	×	N/A	✓	N/A	✓	✓	✓
Proposed	TPC-based	6	6	1	✓	✓	✓	✓	✓	✓	✓

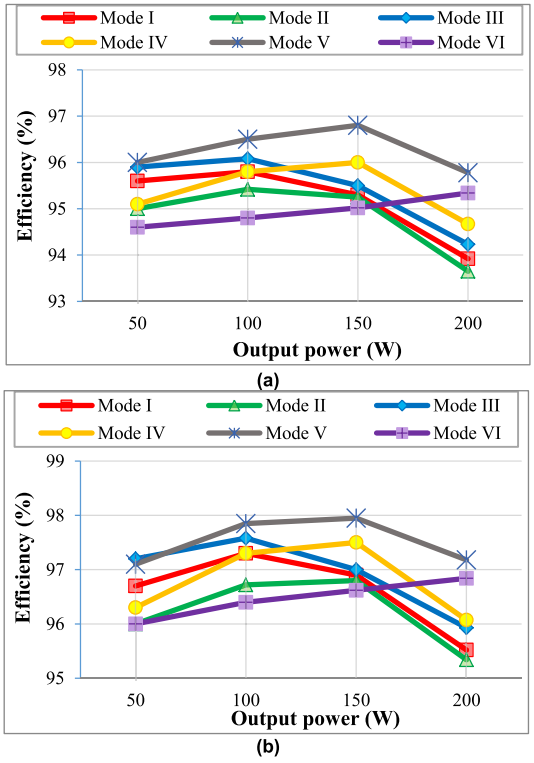

FIGURE 15. Efficiency curves. (a) Hard-switched conventional converter (with the bidirectional power flow path from output to the ESS). (b) Proposed converter.

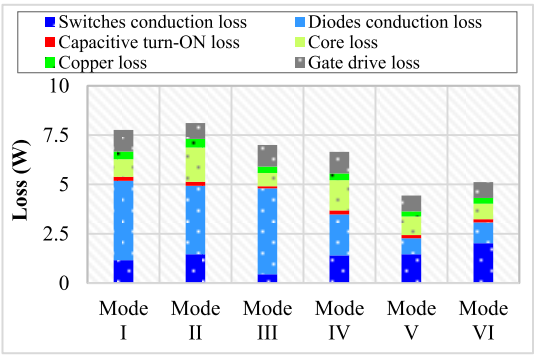

FIGURE 16. Main components loss breakdown of the proposed converter.

indicates that by reducing switching loss, the conduction loss is the dominated loss in the proposed converter.

VI. COMPARISON

In Table 2, the proposed converter is compared with different multi-port converters. At first, in comparison with [9], [19]–[22], [25]–[28], the proposed converter has a bidirectional power flow path to charge ESS from the output. Moreover, the converters introduced in [12], [17], [19]–[22], [28] do not operate under fully soft-switching conditions. In the introduced converter in [21], [22], the switch in the input side of the TPC converter operates under hard-switching condition. And, in [28], the active clamp circuit technique is used to provide soft-switching conditions, and due to the dependency of this technique to output power, the soft-switching condition is missed in Mode III. In the proposed converter, only one magnetic core is used to provide six different operating modes in which, in all of them, the switches operate under soft-switching conditions. However, in [9], [12], [17], [19], [21], [22], [26], [27], [29], more than one magnetic cores are used to have fewer number of operating modes or operate under hard-switching conditions which caused the volume and weight of the converters to be increased.

VII. CONCLUSION

In this paper, a bidirectional multi-port converter with soft-switching capability is proposed. At first, the ESS charging ability from the output port is provided for the conventional three-port converter. Then, a soft-switching cell is used to solve the hard-switching operation of the three-port converter switches which are placed in different power flow paths. Although the power flow paths are changed during different operating modes and each switch has a distinct switching pattern, but the proposed soft-switching conditions are

elaborately provided for all switches under different modes. As a result, by reducing switching loss, the efficiency of the proposed converter is improved in the wide range of the output power. Realizing six distinct operating modes, one-stage power conversion, and soft-switching operation by utilizing only one magnetic core are the prominent advantages in comparison with other counterparts.

REFERENCES

[1] A. Affam, Y. M. Buswig, A.-K.-B. H. Othman, N. B. Julai, and O. Qays, "A review of multiple input DC-DC converter topologies linked with hybrid electric vehicles and renewable energy systems," *Renew. Sustain. Energy Rev.*, vol. 135, Jan. 2021, Art. no. 110186.

[2] Z. Wang, Q. Luo, Y. Wei, D. Mou, X. Lu, and P. Sun, "Topology analysis and review of three-port DC–DC converters," *IEEE Trans. Power Electron.*, vol. 35, no. 11, pp. 11783–11800, Nov. 2020.

[3] S. Bairabathina and S. Balamurugan, "Review on non-isolated multi-input step-up converters for grid-independent hybrid electric vehicles," *Int. J. Hydrogen Energy*, vol. 45, no. 41, pp. 21687–21713, Aug. 2020.

[4] A. H. Chander, L. K. Sahu, S. Ghosh, and K. K. Gupta, "Comparative analysis on selection and synthesis of multiple input converters: A review," *IET Power Electron.*, vol. 13, no. 4, pp. 611–626, Mar. 2020.

[5] W. J. Choy, A. Costabeber, G. Buticchi, A. Trentin, A. Walker, M. Galea, K. Paciura, J. O'Brien, and B. Palmer, "A multiport power electronics converter for hybrid traction applications," *IEEE Access*, early access, Jun. 14, 2021, doi: 10.1109/ACCESS.2021.3089371.

[6] R. Faraji, L. Ding, T. Rahimi, and M. Kheshti, "Application of soft-switching cell with inherent redundancy properties for enhancing the reliability of boost-based DC–DC converters," *IEEE Trans. Power Electron.*, early access, May 19, 2021, doi: 10.1109/TPEL.2021.3081722.

[7] T. Rahimi, L. Ding, R. Faraji, M. Kheshti, J. Pou, and K. H. Loo, "Performance analyses of a three-port converter for post-fault conditions in aerospace applications," in *Proc. 12th Power Electron., Drive Syst., Technol. Conf. (PEDSTC)*, Feb. 2021, pp. 1–6.

[8] M. Pahlevani and P. K. Jain, "Soft-switching power electronics technology for electric vehicles: A technology review," *IEEE J. Emerg. Sel. Topics Ind. Electron.*, vol. 1, no. 1, pp. 80–90, Jul. 2020.

[9] R. Faraji and H. Farzanehfard, "Soft-switched nonisolated high step-up three-port DC–DC converter for hybrid energy systems," *IEEE Trans. Power Electron.*, vol. 33, no. 12, pp. 10101–10111, Dec. 2018.

[10] R. Faraji and H. Farzanehfard, "Fully soft-switched multiport DC–DC converter with high integration," *IEEE Trans. Power Electron.*, vol. 36, no. 2, pp. 1901–1908, Feb. 2021.

[11] G. Chen, Y. Liu, X. Qing, and F. Wang, "Synthesis of integrated multiport DC–DC converters with reduced switches," *IEEE Trans. Ind. Electron.*, vol. 67, no. 6, pp. 4536–4546, Jun. 2020.

[12] B. Chandrasekar, C. Nallaperumal, S. Padmanaban, M. S. Bhaskar, J. B. Holm-Nielsen, Z. Leonowicz, and S. O. Masebinu, "Non-isolated high-gain triple port DC–DC buck-boost converter with positive output voltage for photovoltaic applications," *IEEE Access*, vol. 8, pp. 113649–113666, 2020.

[13] G. G. Kumar, K. Sundaramoorthy, S. Athikkal, and V. Karthikeyan, "Dual input superboost DC–DC converter for solar powered electric vehicle," *IET Power Electron.*, vol. 12, no. 9, pp. 2276–2284, Aug. 2019.

[14] T. Jalilzadeh, N. Rostami, E. Babaei, and S. H. Hosseini, "Multiport DC–DC converter with step-up capability and reduced voltage stress on switches/diodes," *IEEE Trans. Power Electron.*, vol. 35, no. 11, pp. 11902–11915, Nov. 2020.

[15] S. Athikkal, G. G. Kumar, K. Sundaramoorthy, and A. Sankar, "A non-isolated bridge-type DC–DC converter for hybrid energy source integration," *IEEE Trans. Ind. Appl.*, vol. 55, no. 4, pp. 4033–4043, Jul. 2019.

[16] S. Athikkal, G. G. Kumar, K. Sundaramoorthy, and A. Sankar, "Performance analysis of novel bridge type dual input DC–DC converters," *IEEE Access*, vol. 5, pp. 15340–15353, 2017.

[17] K. Varesi, S. H. Hosseini, M. Sabahi, E. Babaei, S. Saeidabadi, and N. Vosoughi, "Design and analysis of a developed multiport high step-up DC–DC converter with reduced device count and normalized peak inverse voltage on the switches/diodes," *IEEE Trans. Power Electron.*, vol. 34, no. 6, pp. 5464–5475, Jun. 2019.

[18] H. Wu, K. Sun, S. Ding, and Y. Xing, "Topology derivation of nonisolated three-port DC–DC converters from DIC and DOC," *IEEE Trans. Power Electron.*, vol. 28, no. 7, pp. 3297–3307, Jul. 2013.

[19] L.-J. Chien, C.-C. Chen, J.-F. Chen, and Y.-P. Hsieh, "Novel three-port converter with high-voltage gain," *IEEE Trans. Power Electron.*, vol. 29, no. 9, pp. 4693–4703, Sep. 2014.

[20] B. Honarjoo, S. M. Madani, M. Niroomand, and E. Adib, "Non-isolated high step-up three-port converter with single magnetic element for photovoltaic systems," *IET Power Electron.*, vol. 11, no. 13, pp. 2151–2160, Nov. 2018.

[21] R. Faraji, E. Adib, and H. Farzanehfard, "Soft-switched non-isolated high step-up multi-port DC–DC converter for hybrid energy system with minimum number of switches," *Int. J. Electr. Power Energy Syst.*, vol. 106, pp. 511–519, Mar. 2019.

[22] R. Faraji, H. Farzanehfard, M. Esteki, and S. A. Khajehoddin, "A lossless passive snubber circuit for three-port DC–DC converter," *IEEE J. Emerg. Sel. Topics Power Electron.*, vol. 9, no. 2, pp. 1905–1914, Apr. 2021.

[23] R. Faraji, H. Farzanehfard, G. Kampitsis, M. Mattavelli, E. Matioli, and M. Esteki, "Fully soft-switched high step-up nonisolated three-port DC–DC converter using GaN HEMTs," *IEEE Trans. Ind. Electron.*, vol. 67, no. 10, pp. 8371–8380, Oct. 2020.

[24] P. Abraham, *Switching Power Supply Design*, 3rd ed. New York, NY, USA: McGraw-Hill, 2009.

[25] R. Faraji, L. Ding, T. Rahimi, M. Kheshti, and M. R. Islam, "Soft-switched three-port DC–DC converter with simple auxiliary circuit," *IEEE Access*, vol. 9, pp. 66738–66750, 2021.

[26] Y. Chen, A. Q. Huang, and X. Yu, "A high step-up three-port DC–DC converter for stand-alone Pv/battery power systems," *IEEE Trans. Power Electron.*, vol. 28, no. 11, pp. 5049–5062, Nov. 2013.

[27] A. T. Harchegani, A. Asghari, and M. Jazaeri, "A new soft-switching multi-input quasi-Z-source converter for hybrid sources systems," *IET Renew. Power Gener.*, vol. 15, no. 7, pp. 1451–1468, May 2021.

[28] G. Zhou, Q. Tian, and L. Wang, "Soft-switching high gain three-port converter based on coupled inductor for renewable energy system applications," *IEEE Trans. Ind. Electron.*, early access, Feb. 25, 2021, doi: 10.1109/TIE.2021.3060614.

[29] A. Hintz, U. R. Prasanna, and K. Rajashekara, "Novel modular multiple-input bidirectional DC–DC power converter (MIPC) for HEV/FCV application," *IEEE Trans. Ind. Electron.*, vol. 62, no. 5, pp. 3163–3172, May 2015.

RASOUL FARAJI (Member, IEEE) received the Ph.D. degree in electronics from the Department of Electrical and Computer Engineering, Isfahan University of Technology, Isfahan, Iran, in 2019.

Also, he was doing part of the Ph.D. dissertation with the École Polytechnique Fédérale de Lausanne (EPFL), Lausanne, Switzerland, as a Visiting Student. Since 2019, he has been a Postdoctoral Researcher with Shandong University, Jinan, China. His research interests include DC–DC switching converters, data analysis using artificial intelligence, implementing algorithms on FPGA, and integrated circuits design. He was a recipient of the Distinguished Researcher Award from the Graduate University of Advanced Technology during his master, in 2012, and the Scholarships from the National Elites Foundation of Iran, in 2013, 2015, and 2017. He was also a recipient of a Visiting Scholarship from the Ministry of Science Research and Technology (Iran) for sabbatical leave at EPFL University, from 2017 to 2018. In 2019, he received Ulam Program Postdoctoral Research Grant sponsored by the Polish National Agency for Academic Exchange (NAWA). Then, he received High-Level Foreign Talents Postdoctoral Fellowship from China Government. Moreover, he won a competitive Grant awarded by China Postdoctoral Science Foundation, in 2020.

LEI DING (Senior Member, IEEE) received the B.E. and Ph.D. degrees in electrical engineering from Shandong University, Jinan, China, in 2001 and 2007, respectively.

From 2008 to 2009, he was a Postdoctoral Researcher with Tsinghua University, Beijing, China. From 2010 to 2011, he was a Research Associate with the University of Manchester. He is currently a Professor with the School of Electrical Engineering, Shandong University. His research interests include power system wide-area protection, low inertia systems, and integration of renewable energy.

TOHID RAHIMI (Member, IEEE) was born in Salmas, Iran. He received the B.Sc. and M.Sc. degrees in electrical engineering, and the Ph.D. degree in system and power electronics from the University of Tabriz, Tabriz, Iran, in 2011, 2013, and 2018. During his Ph.D. course, he was a Teacher Assistant with the University of Tabriz. Also, he was a Supervisor or an Advisor for several M.Sc. theses with the Meraj Higher Education Institute, Iran. He is currently a Postdoctoral Researcher with Shandong University, Jinan, China. He has been served as an active reviewer for different IEEE and other scientific journals. Moreover, he won a competitive grant awarded by China Postdoctoral Science Foundation, in 2020. His interests include power electronics, reliability, EMI, and different fields of power engineering.

HOSEIN FARZANEHFARD (Member, IEEE) was born in Isfahan, Iran, in 1961. He received the B.Sc. and M.Sc. degrees in electrical engineering from the University of Missouri, Columbia, MO, USA, in 1983 and 1985, respectively, and the Ph.D. degree in electrical engineering from Virginia Polytechnic Institute and State University, Blacksburg, VA, USA, in 1992.

Since 1993, he has been a Faculty Member with the Department of Electrical and Computer Engineering, Isfahan University of Technology, Isfahan. He has authored or coauthored more than 200 technical papers published in journals and conference proceedings. His current research interests include high-frequency soft-switching converters, power factor correction, bidirectional converters, active power filters, high-frequency electronic ballasts, and pulse power applications.

HOSSEIN HAFEZI (Member, IEEE) received the B.Sc. degree in electrical engineering from the K. N. Toosi University of Technology, Tehran, Iran, in 2008, the M.Sc. degree in electrical engineering from Dokuz Eylul University, Izmir, Turkey, in 2013, and the Ph.D. degree in electrical engineering from the Energy Department, Politecnico di Milano, Milan, Italy, in 2017. He was a Postdoctoral Research Fellow with the Energy Department, Politecnico di Milano, from January 2017 to May 2018, and an Assistant Professor of electrical engineering with the School of Technology and Innovations, University of Vaasa, Finland, from June 2018 to September 2020. In September 2020, he joined the Faculty of Information Technology and Communication Sciences, Tampere University, as a University Lecturer. His research interests include electric power system studies, power electronics and its applications in power quality improvement and smart grids systems, renewable energies integration into modern and smart grid systems and their effects on power quality and system operation, dc and hybrid dc–ac distribution systems, and microgrid systems.

MOHAMMAD MAGHSOUDI (Member, IEEE) was born in Isfahan, Iran, in 1993. He received the B.Sc. degree in electronics technology engineering from Shahid Mohajer Technical Institute of Isfahan, Isfahan, in 2017. He is currently pursuing the M.Sc. degree in electrical engineering with Isfahan University of Technology (IUT), Isfahan.

His research interests include high-frequency soft-switching converters, power factor correction, and GaN-based converters.